

- **OGLE**
(The optical Gravitational Lensing Experiment)

Collaborators

Dr B. A. Varghese

Prof Diana Kjurkchieva

Mr Valentin

Study of Irradiation Effects in Close Binary Components

M. Srinivasa Rao

April 17-18, 2006

Basic information

What is a binary system ?

Two components of a system which revolve in close elliptical (Or circular) orbits around their common center of gravity.

Binary nature can be discovered in several different ways. From the furthest to the nearest, these are (1) Common Proper Motion Pairs (2) Astrometric Binaries (3) Visual Binaries (4) Eclipsing Binaries (5) Spectroscopic Binaries

Close binary: System of main sequence stars with radii of the order 10% to 15% of their separation falls into this category and reasonably common (for much smaller than this in most cases, hardly any reflection effect).

The close binaries classified into three varieties

(1) **Detached systems** : Both stars well inside Roche lobes
Ex: β Aurigae

(2) **Semi Detached systems** : One star fills its Roche lobe
Ex: Algol (β Persi)

(3) **Contact systems** : Both stars fill their Roche lobes
Ex: 44 Bootis B

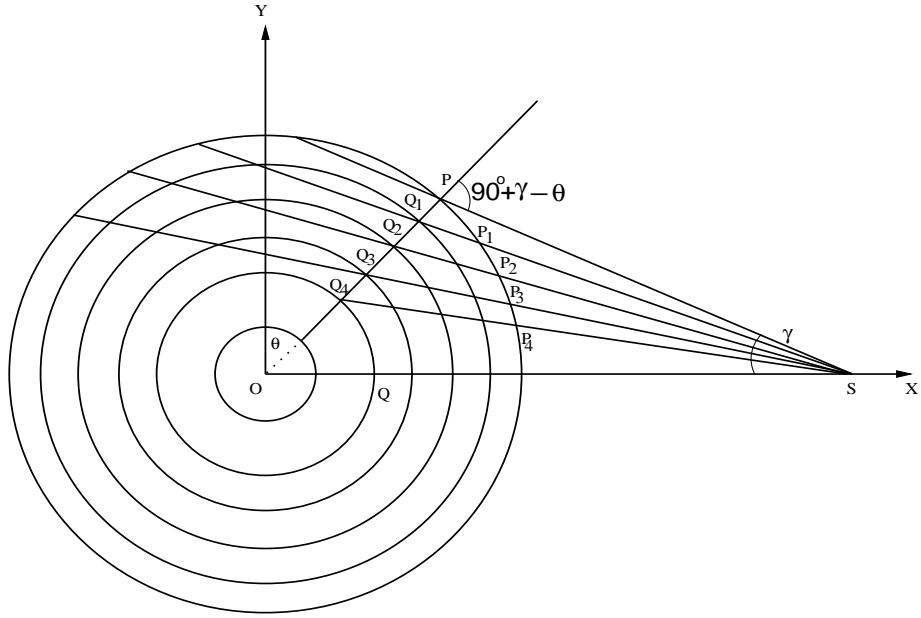
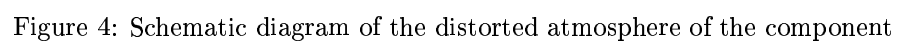
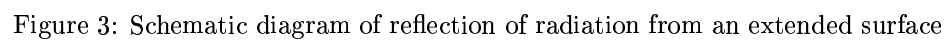
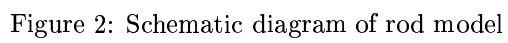


Figure 1: Schematic diagram of reflection of radiation from a point source

Reflection Effect: In a close binary system each component will receive the radiation from its mate (companion) which should evidently heat the side facing the other. If a star is to remain in a radiative equilibrium, it is obvious that all the energy received from outside must be reemitted, without altering the rate of escape from the deep interior. This phenomenon is known as the Reflection effect inevitable in close binaries.

Roche Lobe: The Roche lobe is a mathematically defined surface that exists around each star in a binary system



1 Calculation of irradiation from the secondary component

We shall consider the equation for an equipotential surface of rotating star (or tidally and rotationally distorted surface of a star) is given by Peraiah (1970)

$$\alpha\rho^7\sin^6\theta + \beta\rho^5\sin^4\theta + (\gamma\sin^2\theta + J)\rho^3 - (1 - Q)\rho + 1 = 0 \quad (1)$$

where

$$J = Q(3\sin^2\theta\cos\phi - 1) \quad (2)$$

and θ and ϕ are the colatitude and the azimuthal angles respectively. Further, $\rho = \frac{r}{r_p}$, where r and r_p are the radius at any point on the surface and the radius at the pole respectively and

$$\alpha = \frac{f(X-1)^2}{6X^2} \left(\frac{r_p}{r_e}\right)^7; \quad \beta = \frac{f(X-1)^2}{2X^2} \left(\frac{r_p}{r_e}\right)^5$$

$$\gamma = \frac{f}{2X^2} \left(\frac{r_p}{r_e}\right)^3; \quad Q = \frac{1}{2}\mu \left(\frac{r_p}{r_e}\right)^3; \quad \mu = \frac{m_2}{m_1} \left(\frac{r_e}{R}\right)^3.$$

Here X is the ratio of angular velocities at the equator and pole, f is the ratio of centrifugal to gravity forces at the equator, $\frac{m_2}{m_1}$ is the mass ratio of the two components and $\frac{r_e}{R}$ is the ratio of the radius at the equator to the separation between the centres of gravity of the two components.

Now we shall consider a rotation of a single star. The effects of rotation are to reduce the source function considerably and it is interesting to note that the

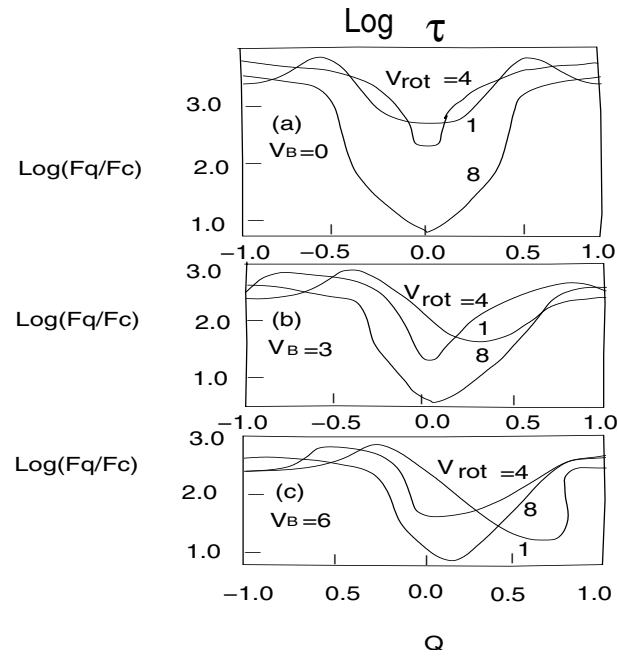
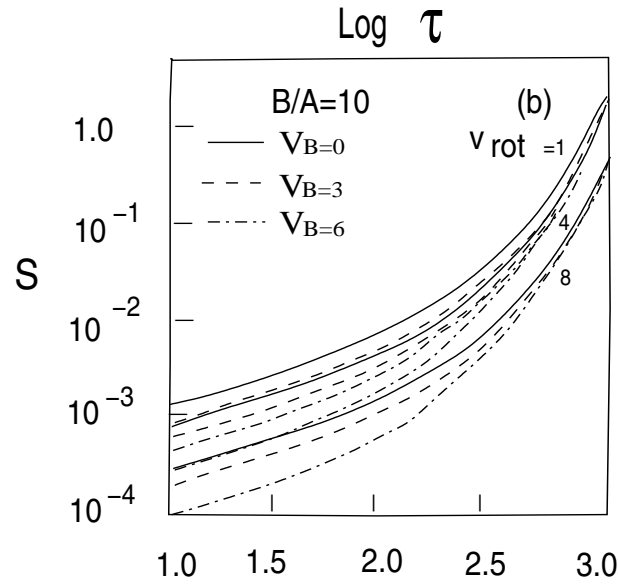
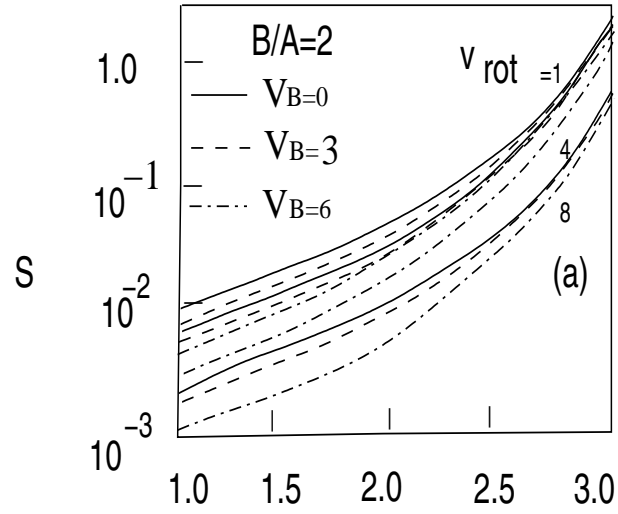


Figure 5: Frequency independent source function in a scattering medium

variation of S runs almost parallel to various velocity gradients. The source functions are reduced considerably when rotational velocities are introduced. The reduction is almost an order of magnitude from $V_{\text{rot}}=1$ to $V_{\text{rot}}=8$. The main reason for dilution is that when rotation increases the equatorial parts tend to extend and the density of radiation field decreases. As we are considering uniform rotation, constant velocity gradients would reduce the radiation field uniformly which explains the reason why the source functions are almost parallel to each other for $V_{\text{rot}}=1, 4$, and 8 .

we obtain a profile with a slight emission in the wings. However when V_{rot} is increased to 4 mean thermal units the wings become boarder whereas the core of the line becomes narrower. When V_{rot} is increased to 8 mtu the lines becomes broader uniformly and emission in the wings disappear. When the expansion velocity increases we find P-Cygni type profile which become more prominent when $V_B = 6$.

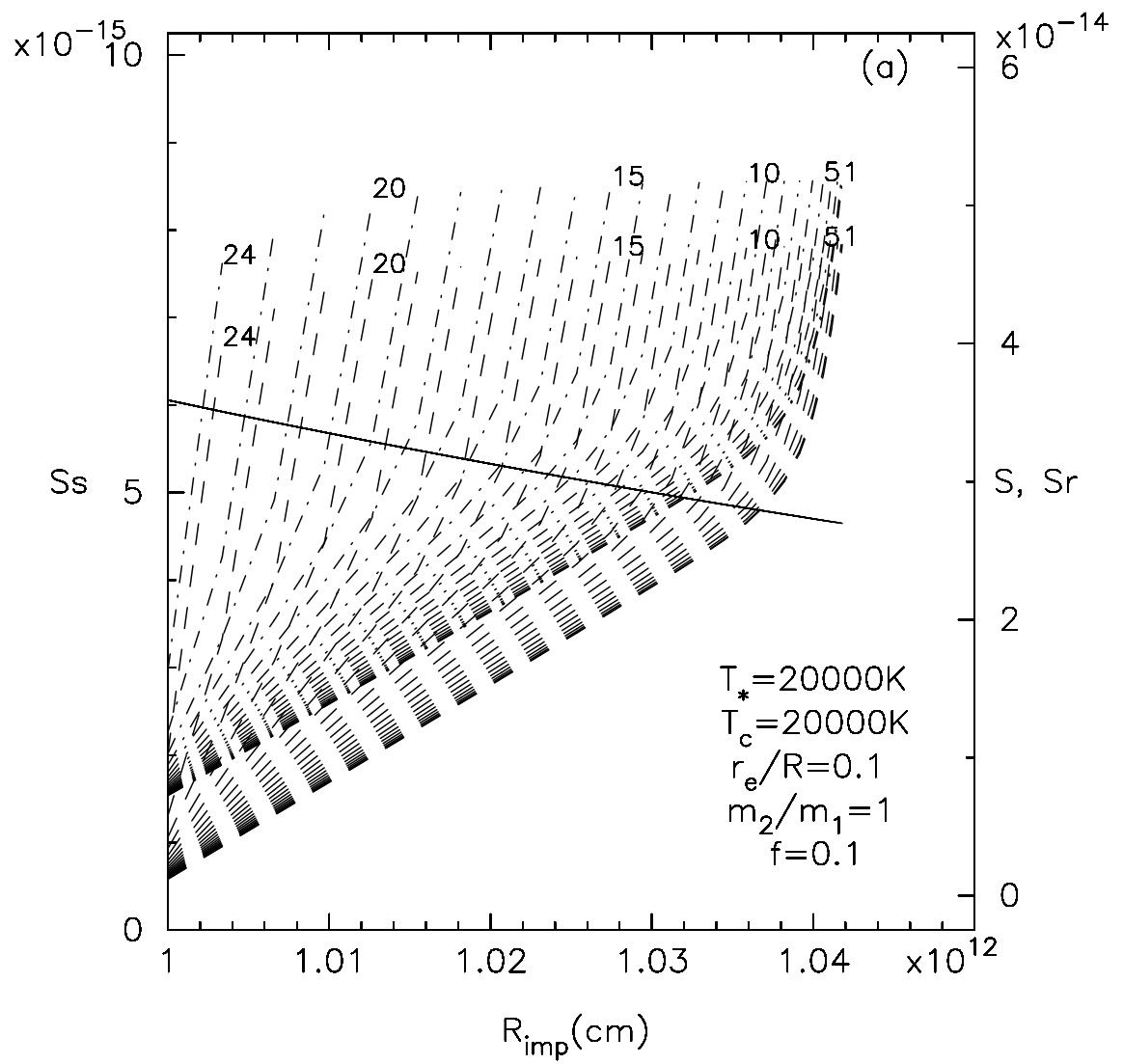


Figure 6: Source functions ar plotted against the distance

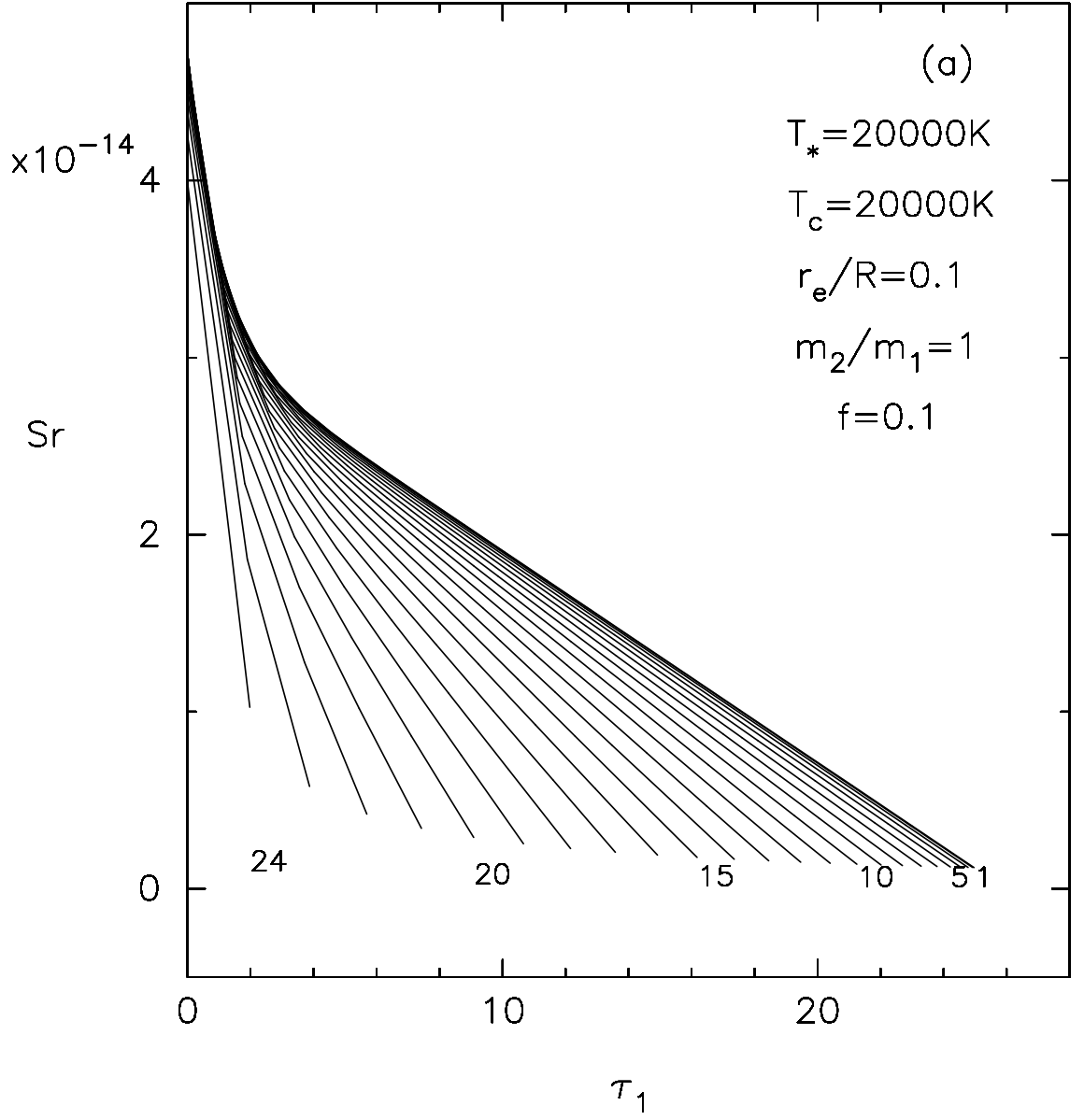


Figure 7: Source functions are plotted against the optical depth

2 Results and discussion

The effects of rotation are to reduce the source function considerably and it is interesting to note that the variation S runs almost parallel to various velocity gradients. The source functions are reduced considerably when rotational velocities are introduced. The reduction is almost an order of magnitude from V_{rot}

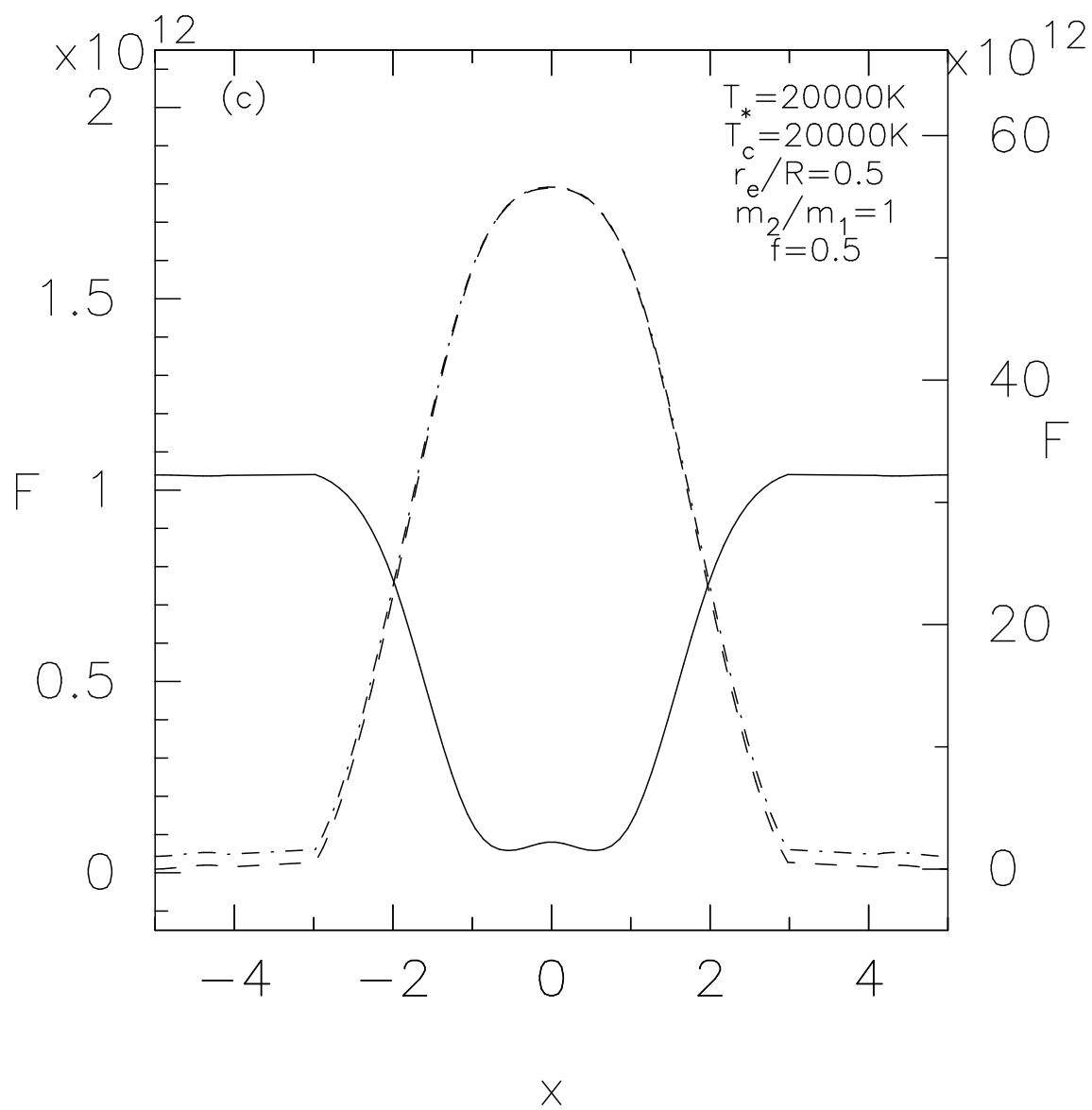


Figure 8: flux profiles are plotted against the normalized frequency

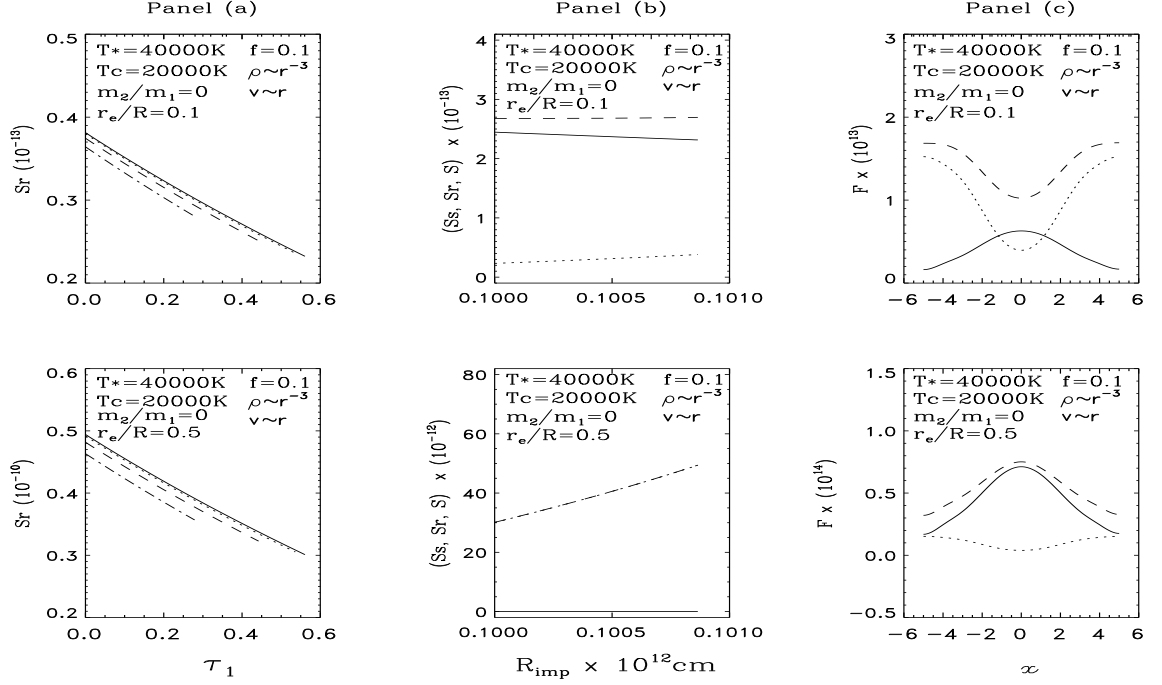


Figure 9: The ray source functions versus the optical depths along the ray for $\frac{r_e}{R} = 0.1, 0.5$. Continuous line for ray 1, dashed line for ray 6, dashed-dotted for ray 12 and dotted line for ray 18 are given above. Panel **a)** $V_A = 0$, $V_B = 0$, Panel **b)** shows the source functions versus R_{imp} plotted for $\frac{r_e}{R} = 0.1, 0.5$. Source functions for self radiation continuous line (S_s), distorted for different source function dashed line of the distorted atmosphere (S_r), total source function (S) dashed - dot. Panel **c)** shows the fluxes against $x = (\nu - \nu_o)/\Delta\nu_D$ where ν_o and ν are the frequency points at the line centre and at any point in the line and $\Delta\nu_D$ is the standard frequency interval such as Doppler width. Fluxes due to self radiation are shown by the continuous line, those due to distorted source function by dotted line, and those due to total source function by the dashed line.

$=1$ to $V_{\text{rot}}=8$. The main reason for dilution is that when rotation increases the equatorial parts tend to extend and the density of radiation field decreases. As we are considering uniform rotation, constant velocity gradients would reduce the radiation field uniformly which explains the reason why the source functions are almost parallel to each other for $V_{\text{rot}}=1, 4$, and 8 . The source functions very similar for $\frac{B}{A} = 2$ and 10 . When the geometrical extension is increased the fall in the source functions corresponding to V_{rot} is large in the case of an atmosphere $\frac{B}{A} = 10$ then that of $\frac{B}{A} = 2$. This is so because we have chosen the same optical depth in both cases and therefore the density in the atmosphere with $\frac{B}{A}=10$ is less than that in the atmosphere with $\frac{B}{A}=2$. This effect is enhanced when the rotational velocities are increased.

In Figs. 3(a) (b) (c) we have presented for $\frac{B}{A}=2$ the line profiles observed at infinity for $V_B=0, 3, 6$ mean thermal units respectively. In each of these figures we have also presented profiles for $V_{\text{rot}}=1, 4, 8$ mean thermal units. In Fig. 3(a) we note that all profiles are symmetric. For $V_{\text{rot}}=1$, we obtain a profile with a slight emission in the wings. However when V_{rot} is increased to 4 mean thermal units the wings become boarder whereas the core of the line becomes narrower. When V_{rot} is increased to 8 mtu the lines becomes broader uniformly and emission in the wings

disappear. When the expansion velocity increases we find P-Cygni type profile which become more prominent when $V_B = 6$ (Fig. 3(c)). In Fig. 4 (a), (b), (c) the flux profiles have been plotted for $\frac{B}{A}=10$. These are similar as given in Fig. 3 (a)(b)(c).

3 Method of calculation

We perform all the calculations in the 3-dimensional X-Y-Z Cartesian geometry as shown in figure 1. We assume a spherical shell of the primary star with inner and outer radii R_{in} and R_{out} respectively. The center of the star is at the origin of coordinates. We assume that radiation is incident from a point source at B moving on a circle of radius R in the X-Z plane. We calculate the radiation field reflected from the spherical shell. We divide the shell into several circular slices such MNPQ parallel to Z-Y plane, with their centers lying on X-axis. We consider the transfer of radiation along the lines such as QS_2RO . Therefore in the X-Y-Z Cartesian coordinate system we should be able to determine the coordinates of any point.

We assume that the secondary component is situated at the point B and a ray from B intersects the outer surface at S_1 and passes through the point S_2 on the line QS_2RO . Let the coordinates of the points S_2 and B (in figure 1) be (x_1, y_1, z_1) and (x_2, y_2, z_2) respectively. The equation of this line is given by

$$\frac{x - x_1}{x_2 - x_1} = \frac{y - y_1}{y_2 - y_1} = \frac{z - z_1}{z_2 - z_1}. \quad (3)$$

By knowing the coordinates of the points S_2 and B in advance, the coordinates of the points S_1 are obtained by solving equation (1) and the equation of the sphere, whose center is at A. The equation

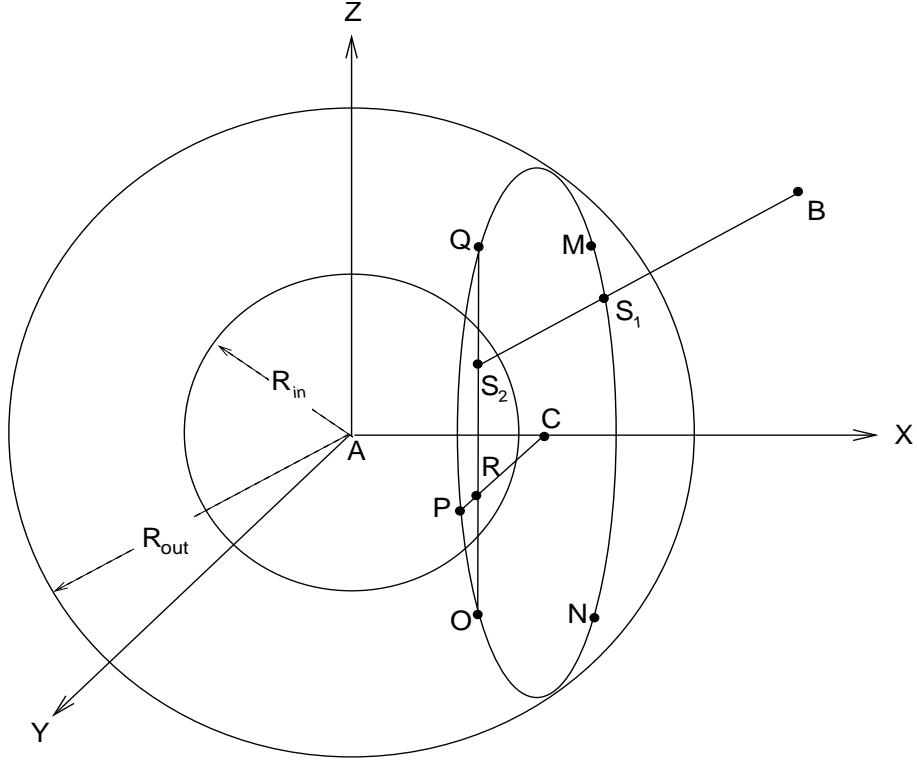


Figure 10: Shows the Schematic diagram of the Cartesian co-ordinate system in X-Y-Z geometry

of the sphere is given by

$$x^2 + y^2 + z^2 = R_{out}^2. \quad (4)$$

The length of the segments are calculated using distance formula. We need to avoid all points where the incident radiation does not reach such as the shadow cone cast by the central star. We calculate the equation of the cone from the enveloping the sphere

$$x^2 + y^2 + z^2 = R_{in}^2. \quad (5)$$

This is given by

$$(x^2 + y^2 + z^2 - R_{in}^2)(x_2^2 + y_2^2 + z_2^2 - R_{in}^2) - (xx_2 + yy_2 + zz_2 - R_{in}^2)^2 = 0. \quad (6)$$

The points that lie in the shadow of this cone should satisfy the relation

$$(x^2 + y^2 + z^2 - R_{in}^2) (x_2^2 + y_2^2 + z_2^2 - R_{in}^2) - (xx_2 + yy_2 + zz_2 - R_{in}^2)^2 \leq 0 \quad (7)$$

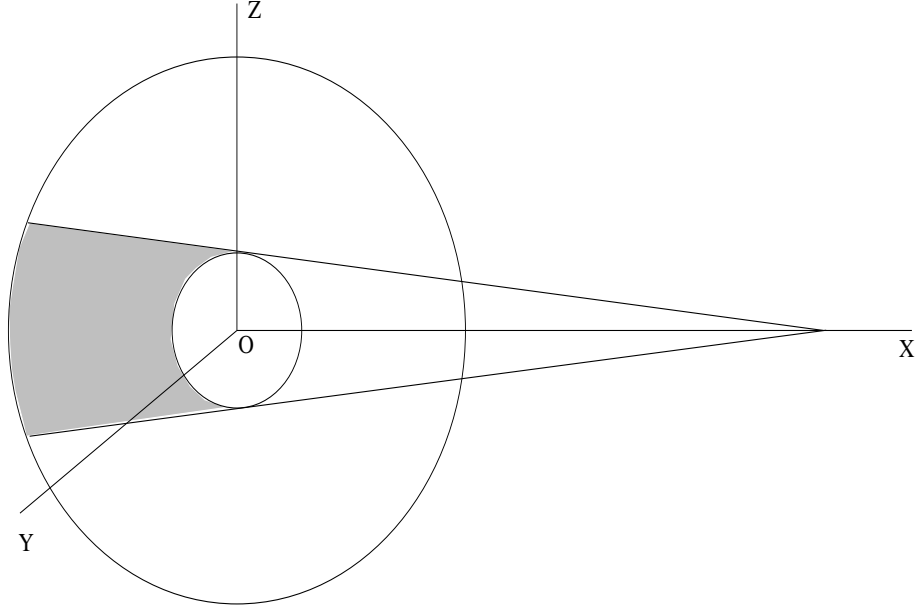


Figure 11: Schemetic diagram of shadow cone casted by the central star

all those points which satisfies the relation are eliminated from calculation.

We estimate the radiation field that is transfered along the line segments such as S_1S_2 to obtain the source function along the lines QS_2RO . We employed the procedure described in Peraiah (1982).

3.1 Calculation of radiation filed due to irradiation

We shall briefly describe the calculation of the source functions derived in the 1-dimensional rod model. The total source function including the diffuse radiation field given by

$$S_d^+(\tau) = S^+(\tau) + \omega(\tau)[p(\tau)I_1e^{-\tau} + (1 - p(\tau))I_2e^{-(T-\tau)}], \quad (8)$$

$$S_d^-(\tau) = S^-(\tau) + \omega(\tau)[(1 - p(\tau))I_1e^{-\tau} + p(\tau)I_2e^{-(T-\tau)}], \quad (9)$$

where $S^+(\tau)$ and $S^-(\tau)$ are the source functions at the optical depth τ (for details see Peraiah (1982)). $\omega(\tau)$ is the albedo for single scattering and p is the phase function equal to $\frac{1}{2}$ in this case. We set $\omega(\tau) = 1$ which corresponds to pure scattering in the medium.

I_1 and I_2 are the incident specific intensities at the boundaries at $\tau = 0$ and $\tau = T$ respectively. For isotropic scattering $S_d^+ = S_d^-$ and equation (6) and (7) will reduce to

$$S_r = \frac{1}{2}[I^+ + I^-] + \frac{1}{2}[I_1 e^{-\tau} + I_2 e^{-(T-\tau)}], \quad (10)$$

where T is the total optical depth at the point where the source function is calculated. We set $\tau = 0$ at point S_1 (see figure 1) where the incident ray enters the medium, and we set $\tau = T$ at the point S_2 where the source function is calculated.

$$I^+(\tau) = I_1 \frac{1 + [T - \tau][1 - p]}{1 + T[1 - p]}, \quad (11)$$

and

$$I^-(\tau) = I_1 \frac{[T - \tau][1 - p]}{1 + T[1 - p]}, \quad (12)$$

$$I^-(\tau = T) = 0 = I_2, \quad (13)$$

$$I^+(\tau = 0) = I_1, \quad (14)$$

therefore

$$I^+(\tau = T) = I_1 \frac{1}{1 + \frac{1}{2}T}, \quad (15)$$

$$I^-(T) = 0, \quad (16)$$

At $\tau = T$, the source function becomes,

$$S_r = \frac{1}{2}[I^+ + I^-] + \frac{1}{2}[I_1 e^{-T}]. \quad (17)$$

Introducing equation (9) and (10) into the above equation with $p = \frac{1}{2}$, we obtain

$$S_r = \frac{1}{2}I_1 \left[\frac{2}{2 + T} + e^{-T} \right]. \quad (18)$$

Using the above analysis we can calculate the source functions according to one-dimensional rod model.

In addition to the irradiation from the secondary component we have the radiation from the primary star itself. In the next section we shall describe method of calculation of self radiation of the primary component.

3.2 Calculation of self radiation of the primary component

The radiative transfer equation in a spherically symmetric approximation is

$$\mu \frac{\partial I(r, \mu)}{\partial r} + \frac{1}{r} \frac{\partial}{\partial \mu} \left[(1 - \mu^2) I(r, \mu) \right] + \sigma(r) I(r, \mu) = \sigma(r) [S_s(r) - I(r, \mu)], \quad (19)$$

where

$$S_s(r) = \frac{1}{2} \int_{-1}^{+1} p(r, \mu, \mu') I(r, \mu') d\mu'. \quad (20)$$

Here $I(r, \mu)$ is the specific intensity of the ray making an angle $\cos^{-1} \mu$ with the radius vector. The quantities $\sigma(r)$ and $S_s(r)$ are the absorption coefficient and the source function respectively and $P(r, \mu, \mu')$ is the phase function for isotropic scattering and function is normalised such that

$$\frac{1}{2} \int_{-1}^{+1} p(r, \mu, \mu') I(r, \mu') d\mu' = 1 \quad (21)$$

and $p(r, \mu, \mu') \geq 0$ and $-1 \leq \mu, \mu' \leq 1$

3.3 Brief description of the numerical method for solving the radiative transfer equation in spherical symmetry

The solution of radiative transfer equation (17) in spherical symmetry is developed by using discrete space theory of radiative transfer Peraiah and Grant (1973). In general the following steps are followed for obtaining the solution.

- (i) We divide the medium into a number of "cells" whose thickness is less than or equal to the critical (τ_{crit}). The critical thickness is determined on the basis of physical characteristics of the medium. τ_{crit} ensures the stability and uniqueness of the solution.
- (ii) Now the integration of the transfer equation is performed on the "cell" which is two-dimensional radius - angle grid bounded by $[r_n, r_{n+1}] \times [\mu_{j-\frac{1}{2}}, \mu_{j+\frac{1}{2}}]$ where $\mu_{j+\frac{1}{2}} = \sum_{k=1}^j C_k$, $j = 1, 2, \dots, J$, where C_k are the weights of Gauss Legendre formula.
- (iii) By using the interaction principle described in Peraiah and Grant (1973), we obtain the reflection and transmission operators over the "cell".
- (iv) Finally we combine all the cells by the star algorithm described in Peraiah and Grant (1973) and obtain the radiation field.

3.4 Boundary conditions

The boundary conditions are assumed as follows

$$U_{N+1}^-(\tau = T, \mu_j) = 1 \quad \text{for all } \mu'_j s \quad (22)$$

$$U_1^+(\tau = 0, \mu_j) = 0 \quad \text{for all } \mu'_j s \quad (23)$$

Equation (20) represents the incident radiation on the atmosphere where the radius is minimum, and equation (21) represents the boundary condition at maximum radius, for $\omega = 1$.

3.5 Calculation of total source function

If $J(r)$ is the mean intensity then the total source function $S_T(x, y, z)$ is given by

$$S_T(x, y, z) = S_r(x, y, z) + J(x), \quad (24)$$

this means that total source function (S_T) is sum of the source functions due to self radiation of the primary star (S_s) and the irra-

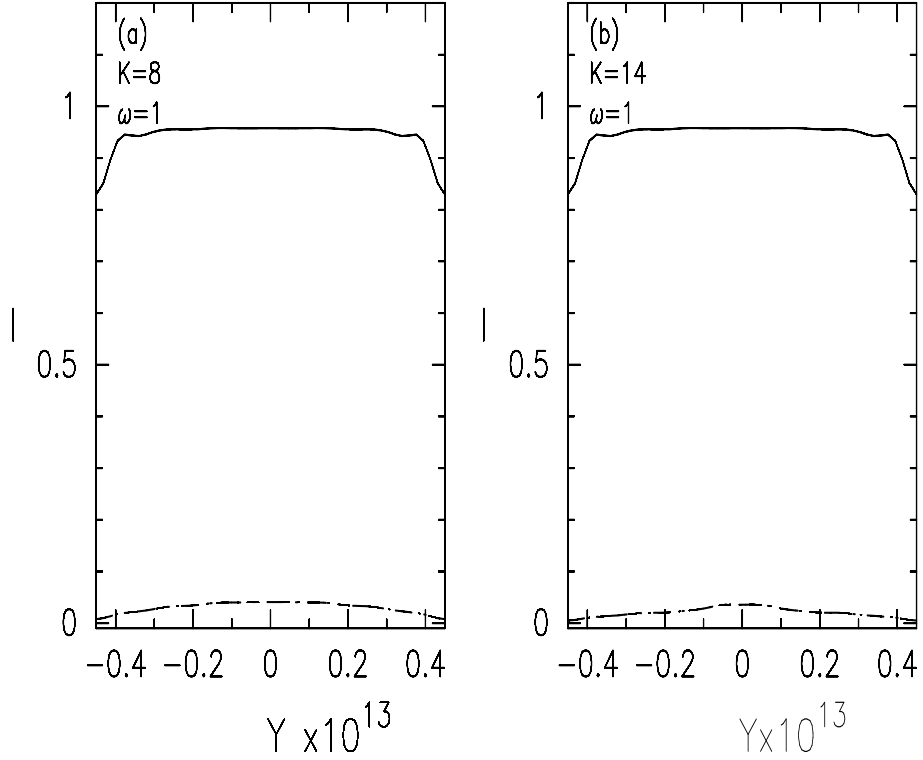


Figure 12: Shows the comparison of self radiation represented by line dash, reflected radiation represented by the line dash dot and the total radiation is represented by continuous line along the Y-axis in case 1

diation from the secondary component which is assumed as point source (S_r).

4 Brief description of the computational procedure

We have used the following data:

$R_{\text{in}} = 10^{12}\text{cm}$, $R_{\text{out}} = 5 \times 10^{12}\text{cm}$, $R=10^{13}\text{cm}$ where R_{in} , R_{out} is the inner and outer radius of the primary star and R is the separation between two components. We assumed a constant electron density of 10^{12}cm^{-3} . As mentioned earlier, we calculate the intensities along the lines such as QS_2RO in a given circular slice. These slices are designed as $K= 1, 2, 3, \dots$ where the slice with designed $K= 1$ corresponds to that at $x = R_{\text{out}}$, that with $K= 11$ corresponds to that at $x = 0$ and that with $K= 21$ corresponds to that at $x = -R_{\text{out}}$. We give unit incident intensity at the surface $r =$

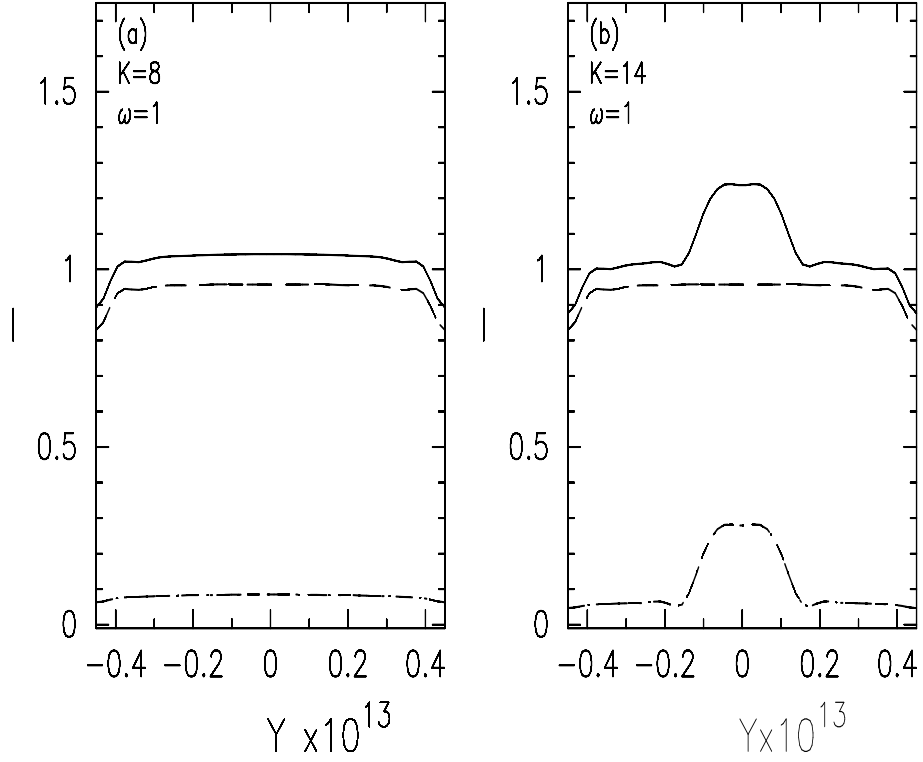


Figure 13: Shows the comparison for case2. The notation is same as case 1

R_{out} . We set the secondary component coordinates which is a point source as (x_2, y_2, z_2) where the radiation is incident on the primary component. We consider the following, cases and calculate the direction cosines of the lines which are parallel to the Z-axis and also parallel to the line of sight. We can consider many number of cases keeping secondary component in different positions in a circular orbit. We can obtain many possible cases but we consider following cases.

Case 1: $x_2 = R$, $y_2 = 0$, $z_2 = 0$;

Case 2: $x_2 = R \sin \frac{\pi}{4}$, $y_2 = 0$, $z_2 = R \cos \frac{\pi}{4}$; and

Case 3: $x_2 = 0$, $y_2 = 0$, $z_2 = R$.

In the above cases we have placed the secondary component on the X-axis at a distance R in case 1 i.e., $(x_2 = R, y_2 = 0, z_2 = 0)$; In case 2, the secondary component is placed between X and Z axis as the line making 45° with X-axis i.e., $(x_2 = R \sin \frac{\pi}{4}, y_2 = 0, z_2 = R \cos \frac{\pi}{4})$; and in case 3, the secondary component is placed on

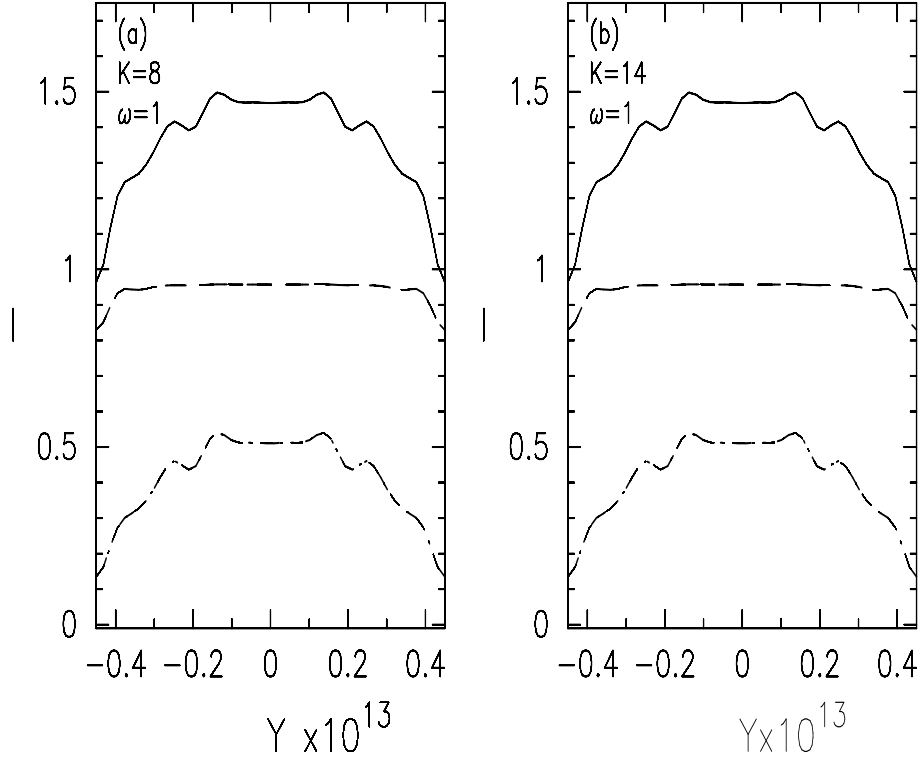


Figure 14: Shows the comparison for case3. The notation is same as case 1

the Z-axis with distance of R i.e., $(x_2 = 0, y_2 = 0, z_2 = R)$.

5 Results and Discussion

Using the above mentioned data we have plotted figures 2 to 4 reflected radiation represented by dash dot line, self radiation represented by dash dash line and total radiation is denoted by continuous line for $K= 8, 14$ in a scattering medium along Y-axis. In all the above three cases we observe that the self radiation is same and also it is constant throughout the atmosphere of the primary component and also decreases towards the limb.

Case 1: In figure 2(a, b) the irradiation from the secondary component is small, when compared to the self radiation of the primary star. This is due to the fact that we have considered secondary component as a point source which is at a distance of $R= 10^{13}$ cm from the primary component. The contribution of reflected radiation is

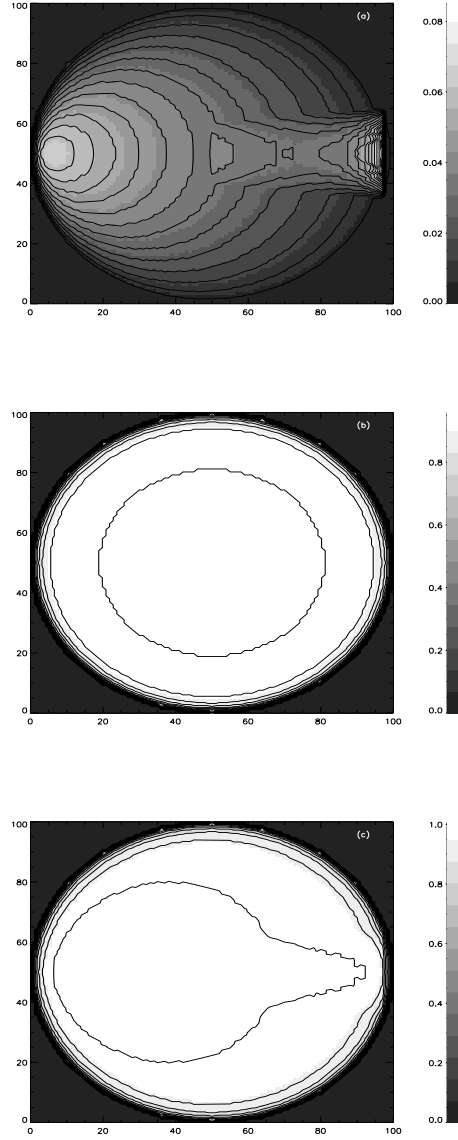


Figure 15: Shows the contour plot for case1 for (a) reflected radiation (b) self radiation (c) total radiation

small and there is no quantitative differences between self radiation and the total radiation curves in the figure 2(a, b) for $K=8$ and 14. So self radiation is dominating factor in this case but still the effect of irradiation can not be neglected. We can see the effect of irradiation in figure 5(a, b, c).

The surface of for primary component shows changes in intensity in figure 5(b). We also can observe irradiation effect on the primary component in figure 5(a) facing the secondary component. This happens because the atmosphere of the star with a close companion

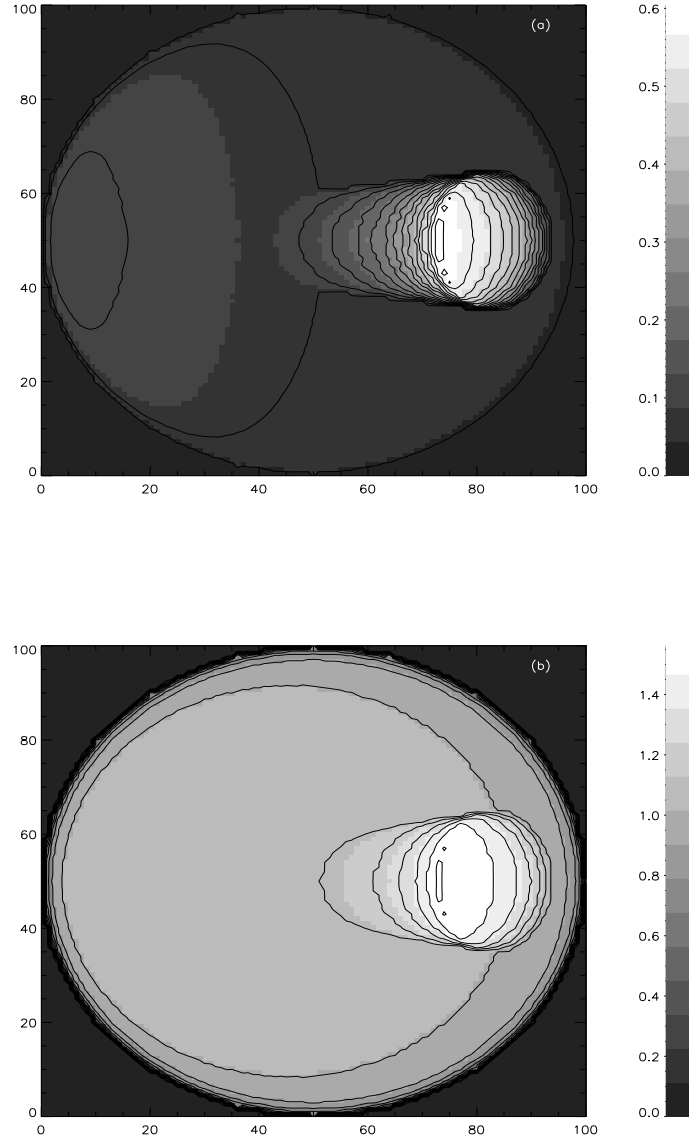


Figure 16: shows contour map for (a) reflected and (b) total radiation for case 2

is influenced by two interaction mechanisms 1) gravitational interaction results in a distortion of the outer layers of the star and 2) the radiative interaction results in a warming of surface layers. So we observe intensity variation in figure 5(a). Figure 5(c) shows the brightness distribution of the total radiation (self+irradiation). Case 2: In figure 3(a, b) we can see the reflected radiation is almost constant in the atmosphere of the primary component and considerable amount of irradiation is added from the secondary component to the self radiation of the primary component in figure 3(a). The

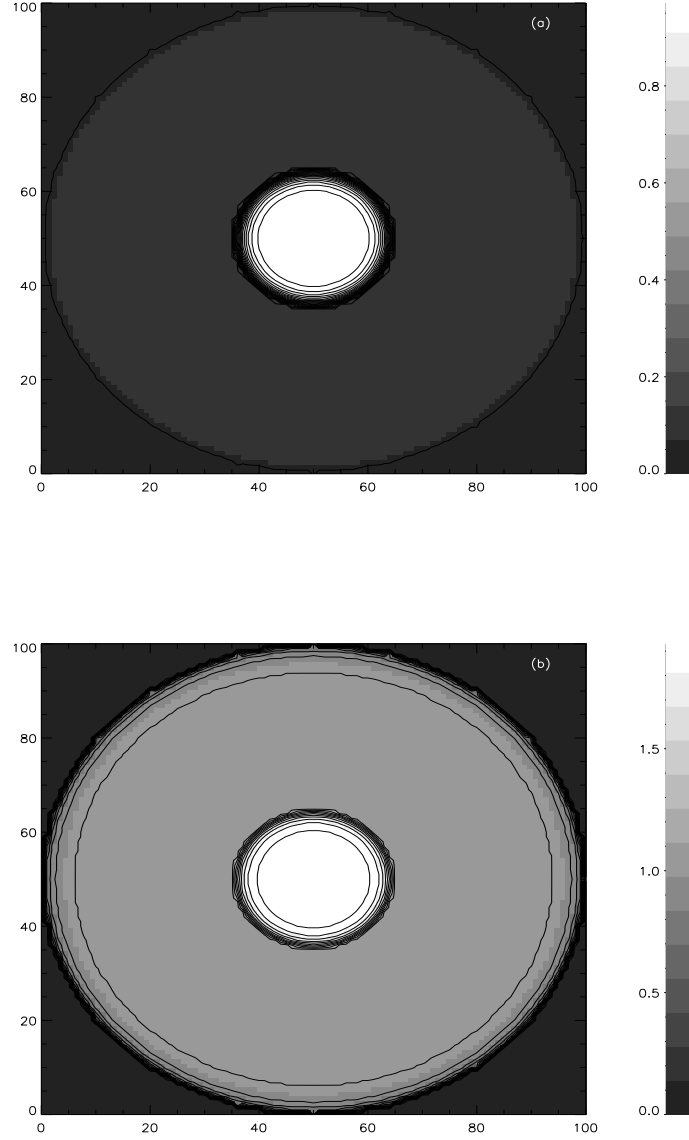


Figure 17: shows contour map for (a) reflected and (b) total radiation for case 3

total radiation behaves as the self radiation, but one can clearly see the curves are separated in figure 3(a) because irradiation contributed more substantially.

In figure 3(b) we see that reflected radiation is stronger in the range $|Y| \leq 0.2$ than outside this range and contribute significant amount of radiation going towards the center of the star due to scattering processes and is a dominating factor in that range. The total radiation almost behaves like reflected radiation in the range $|Y| \leq 0.2$. While modeling the close binary system one should not neglect the

irradiation effect which plays an important role.

We also can observe similar features in contour maps of figure 6(a, b) which shows reflected and total radiation. Due to the angle of incidence, the shadow cone casted by the central star is changed and also. brightness distribution is shown in figure 6(a) and total radiation in 6(b).

Case 3: In figure 4(a, b) we see that $K=8$ and $K=14$ the reflected, self and total radiation is same by symmetry. In comparison with case1 and case2 the reflected radiation is more in this case. This is because primary component receives the radiation directly from the secondary. We also can observe that intermediate regions have combined radiation (ie., irradiation which is coming towards the centre of the star and the self radiation of the primary star) filed. So due to this reason the maximum radiation is occurs central regions primary component. We also plotted the contour for reflected and for total radiation distribution in this case in figure 7(a, b).

6 Conclusions

- While modeling binary sytem reflection effect has to be considered.
- This effect place an important role on spectral lines
- Proximity of secondary is important because as it close to the primary it contribute more radiation
- Position of the secondary important

7 future work

We would like to study the irradiation effects when secondary component is an extended surface and the effect of gravity darkening in a binary system in XYZ-geometry.

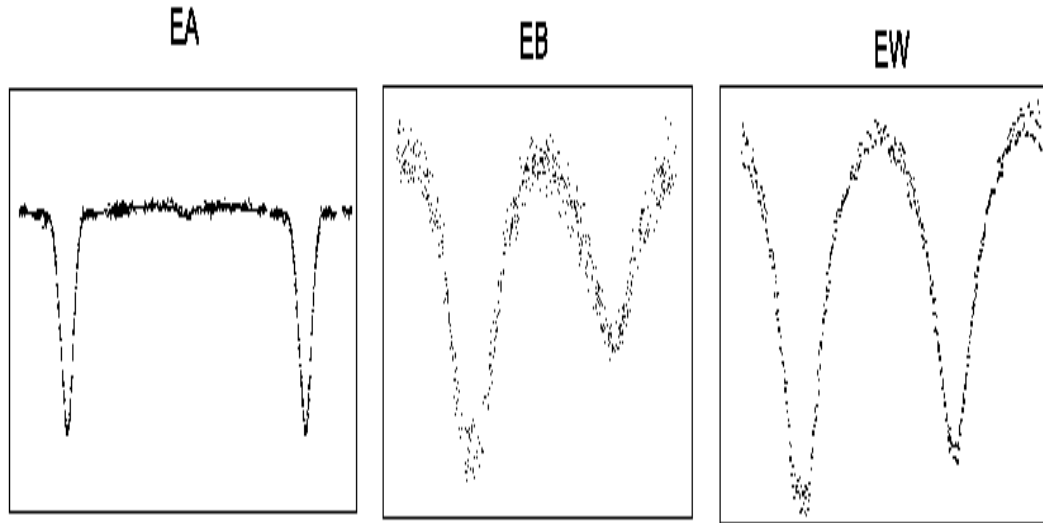


Figure 18: Light curves

8 OGLE Data

OGLE (The optical Gravitational Lensing Experiment). The Photometric data of 2580 binary stars were collected during 1997 - 2000. Eclipsing binary stars are among the most important sources of information on stellar parameters like mass, radius, luminosities etc. The detected data of eclipsing binary were divided into three classical types.

EA ——— (Algol type) (Spherical or slightly ellipsoidal components)

EB ——— (β Lyr type) (Ellipsoidal components)

EW ——— (W Uma type) (Ellipsoidal components periods are shorter than 1 day) These type of contact binary stars are surprisingly common in the solar neighborhood

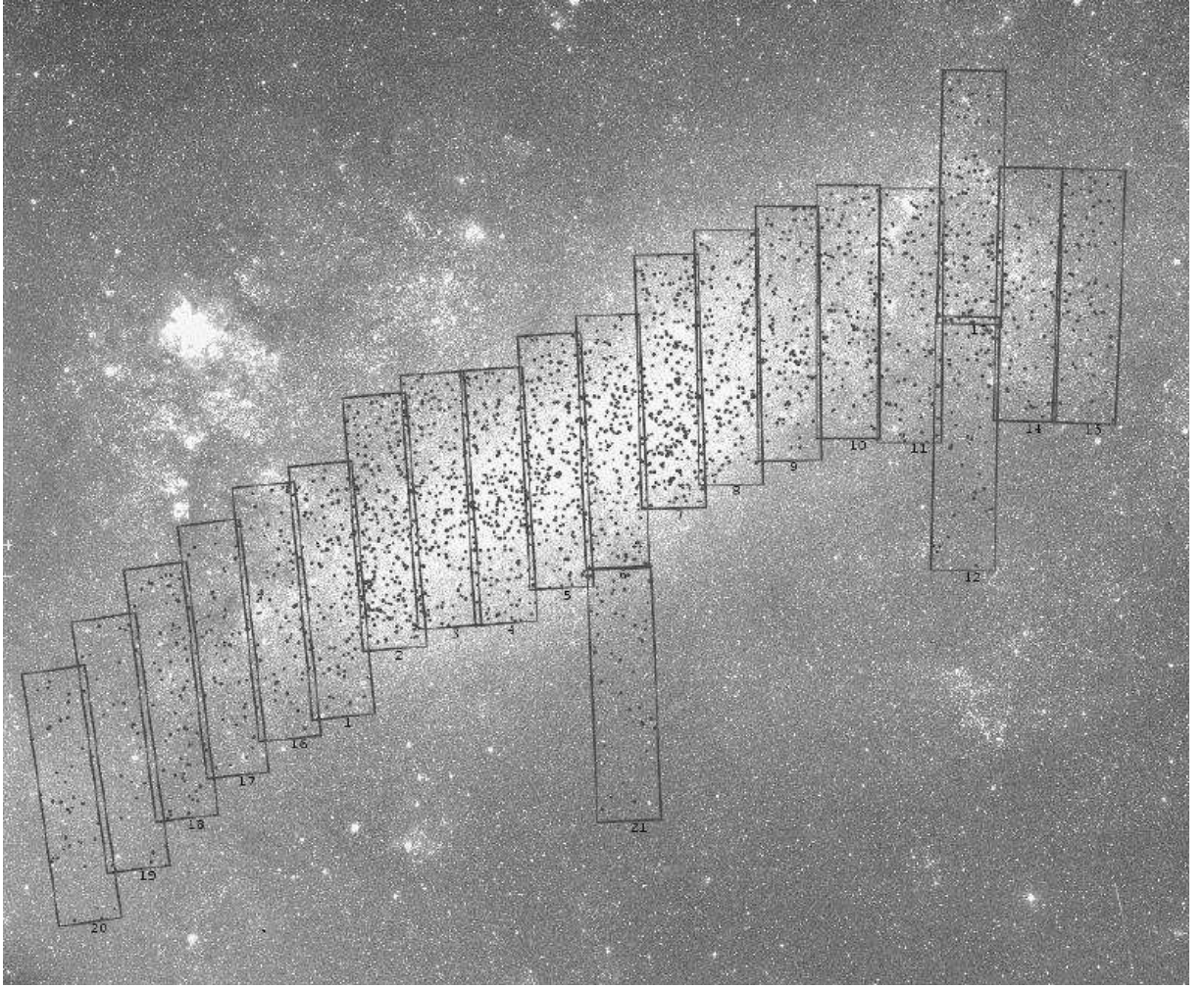


Figure 19: OGLE II fields in the LMC. Dots include positions of eclipsing stars. North up and East to left in the Digitized sky survey (DSS)

The data analysis is in the following way:

- 1) We have to choose good light curve with secondary minimum at the phase at 0.5
- 2) We have begin with I, B, V data, if it has a mini-um number of data points select that data. In this case we have chosen only I data because B and V data have not sufficient points.
- 3) The data have to be phased
- 4) We have to convert the data into flux. So finally we have the data (Phase, flux). Using some software package (Binmaker2) I could produce the synthetic light curve.
- 5) As a final step I have to feed this data in Wilson, R. E, Devinney,

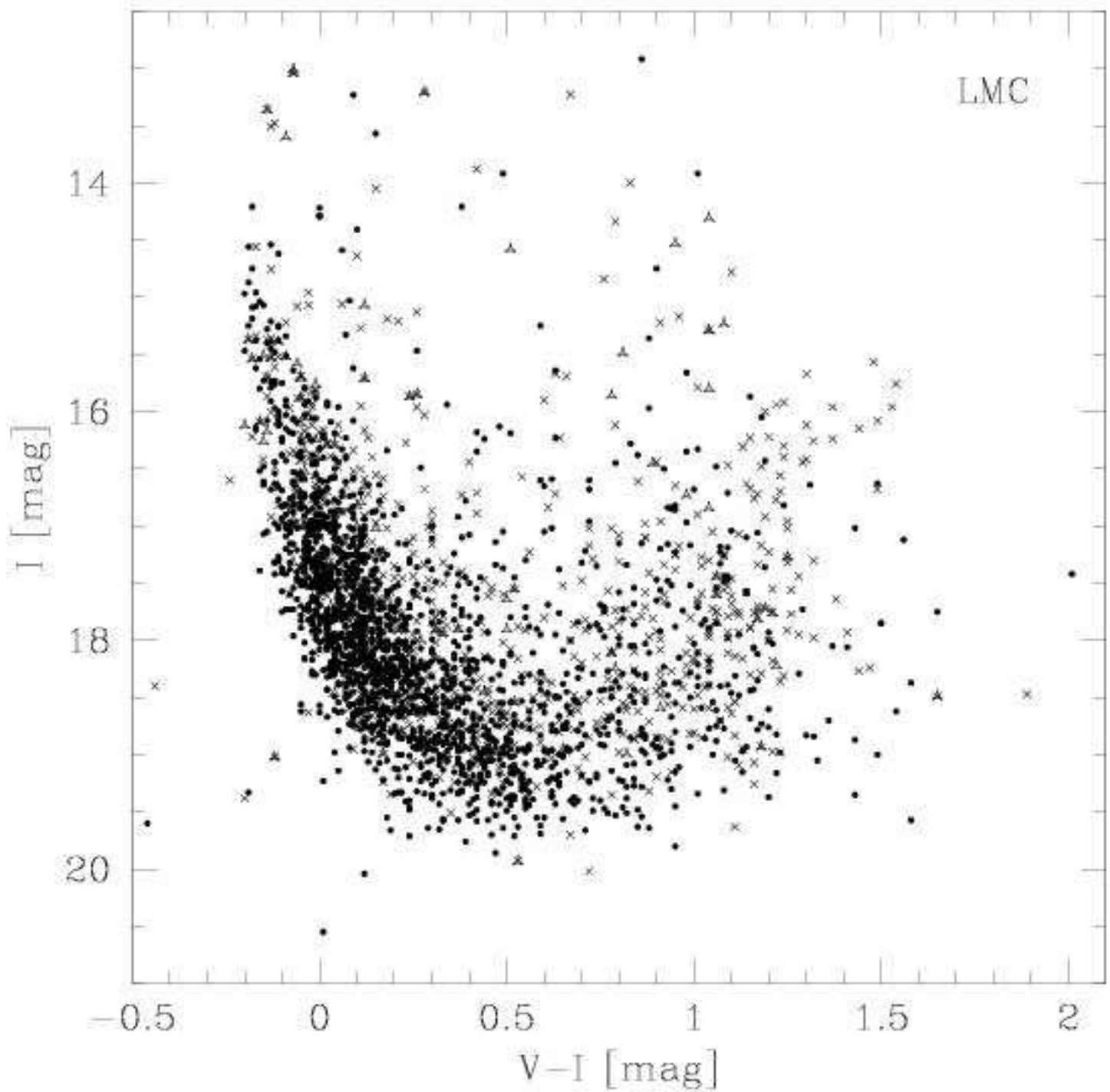


Figure 20: Colour-magnitude diagram of eclipsing binaries in the LMC. Solid dots, crosses and triangle mark EA, EB, and EW type objects respectively

No.	Field	Star	RA	DEC	X_{ref}	Y_{ref}	$P(d)$	T_0 JD-2450000	I_{max}	Ampl I(mag)	Sec. Ecl Phase	Sec. Ecl Depth I(mag)	V_{depth}	B_{depth}	Type	Notes
1	LMC_SC1	CG LEO 332 27 36 -70 11 48.4	03:32:27.36	-70:11:48.4	24.037	32.69433	1.543800	-435.43870	18.71	0.61	0.31	0.34	18.67	18.16	-	Overlaps with LMC_SC2
2	LMC_SC1	CG LEO 332 30 70 -70 08 38.3	03:32:30.70	-70:08:38.3	62.913	37.28326	3.696430	-435.43331	18.19	0.08	0.30	0.41	18.19	18.63	EA	Overlaps with LMC_SC2
3	LMC_SC1	CG LEO 332 32 35 -70 06 36.3	03:32:32.35	-70:06:36.3	74.001	-45.4406	1.223200	-434.91971	17.39	0.23	0.31	0.14	17.38	17.69	EA	-
4	LMC_SC1	CG LEO 332 34 48 -70 02 18.2	03:32:34.48	-70:02:18.2	102.328	-46.47261	1.377030	-435.67840	18.17	0.44	0.30	0.38	18.16	18.33	EA	Overlaps with LMC_SC2
5	LMC_SC1	CG LEO 332 35 27 -70 26 06.7	03:32:35.27	-70:26:06.7	134.123	11.96473	1.663430	-436.09560	17.41	0.19	0.34	0.14	17.39	17.44	EA	-
6	LMC_SC1	CG LEO 332 36 23 -70 06 44.3	03:32:36.23	-70:06:44.3	128.498	-80.4248	2.639240	-437.37322	17.37	0.22	0.48	0.16	17.27	17.38	EA	-
7	LMC_SC1	CG LEO 332 36 30 -69 54 03.7	03:32:36.30	-69:54:03.7	123.991	38.36188	3.617800	-432.71699	17.78	0.26	0.31	0.23	17.38	17.28	EA	Overlaps with LMC_SC2
8	LMC_SC1	CG LEO 332 36 37 -70 03 17.1	03:32:36.37	-70:03:17.1	134.329	-40.93124	1.549470	-434.32310	18.92	1.11	0.31	0.34	18.79	19.01	EA	Overlaps with LMC_SC2
9	LMC_SC1	CG LEO 332 38 06 -70 13 54.2	03:32:38.06	-70:13:54.2	164.306	29.66403	3.481640	-433.44323	17.36	0.27	0.30	0.24	17.32	17.47	EA	Overlaps with LMC_SC2
10	LMC_SC1	CG LEO 332 40 31 -70 11 27.8	03:32:40.31	-70:11:27.8	182.681	33.20101	1.903630	-436.39061	18.16	1.43	0.31	0.41	18.21	18.46	EA	-
11	LMC_SC1	CG LEO 332 41 43 -69 41 49.3	03:32:41.43	-69:41:49.3	171.447	70.16323	13.642300	-491.06174	17.37	0.13	0.32	0.14	17.36	18.33	EA	-
12	LMC_SC1	CG LEO 332 41 03 -69 31 09.2	03:32:41.03	-69:31:09.2	183.401	62.63737	4.934340	-433.39493	16.93	0.34	0.48	0.30	16.91	16.87	EA	-
13	LMC_SC1	CG LEO 332 42 43 -70 03 13.3	03:32:42.43	-70:03:13.3	208.383	-42.54363	0.938740	-433.71161	18.00	0.31	0.30	0.29	17.79	18.19	EA	-
14	LMC_SC1	CG LEO 332 44 07 -69 54 06.8	03:32:44.07	-69:54:06.8	214.383	38.34310	2.314920	-433.76774	18.64	0.47	0.31	0.41	18.63	19.02	EA	-
15	LMC_SC1	CG LEO 332 44 70 -70 16 21.3	03:32:44.70	-70:16:21.3	241.741	36.10919	3.047380	-432.04023	19.13	1.31	0.31	0.41	19.14	19.92	EA	-
16	LMC_SC1	CG LEO 332 47 34 -69 40 03.1	03:32:47.34	-69:40:03.1	230.030	72.93340	0.331033	-434.77707	16.47	0.42	-	-	16.43	17.34	EA	-
17	LMC_SC1	CG LEO 332 48 27 -70 30 13.0	03:32:48.27	-70:30:13.0	293.301	60.2169	1.113930	-433.09168	18.91	0.73	0.31	0.26	18.84	19.01	EA	-
18	LMC_SC1	CG LEO 332 48 77 -69 54 43.3	03:32:48.77	-69:54:43.3	286.131	37.41835	3.749730	-434.60472	16.88	0.69	0.30	0.16	16.86	16.94	EA	-
19	LMC_SC1	CG LEO 332 51 37 -70 14 46.9	03:32:51.37	-70:14:46.9	321.180	38.39980	6.162960	-430.94134	18.39	0.79	0.49	0.34	18.33	18.94	EA	-
20	LMC_SC1	CG LEO 332 51 73 -70 02 36.2	03:32:51.73	-70:02:36.2	316.633	-43.36781	0.297173	-434.67083	16.73	0.77	0.30	0.60	16.73	17.71	EA	-
21	LMC_SC1	CG LEO 332 52 71 -69 48 37.6	03:32:52.71	-69:48:37.6	318.336	36.30723	6.964140	-434.61819	17.91	0.23	0.31	0.21	18.40	19.41	EA	-
22	LMC_SC1	CG LEO 332 53 08 -69 38 37.9	03:32:53.08	-69:38:37.9	334.998	31.90730	0.901480	-433.28013	18.74	0.63	0.30	0.39	18.64	18.96	EA	-
23	LMC_SC1	CG LEO 332 57 00 -70 06 38.3	03:32:57.00	-70:06:38.3	393.830	39.1376	1.289960	-436.12106	18.60	0.64	0.30	0.38	18.39	18.84	EA	-
24	LMC_SC1	CG LEO 332 58 41 -70 11 52.3	03:32:58.41	-70:11:52.3	417.686	32.62333	3.738280	-431.11831	19.12	1.39	0.30	0.32	19.08	19.39	EA	-
25	LMC_SC1	CG LEO 332 59 07 -69 36 38.6	03:32:59.07	-69:36:38.6	414.380	34.67233	3.368130	-436.82108	17.34	1.39	0.30	0.26	17.31	17.41	EA	-
26	LMC_SC1	CG LEO 333 00 70 -70 19 24.1	03:33:00.70	-70:19:24.1	438.779	21.46773	1.839130	-433.32318	18.48	0.93	0.31	0.28	18.43	18.72	EA	-
27	LMC_SC1	CG LEO 333 01 16 -70 08 03.4	03:33:01.16	-70:08:03.4	476.727	38.10443	3.540010	-431.84411	18.70	0.39	0.30	0.36	18.69	19.43	EA	-
28	LMC_SC1	CG LEO 333 02 18 -70 02 37.1	03:33:02.18	-70:02:37.1	443.743	-40.93312	2.649780	-437.21649	18.70	0.82	0.30	0.78	18.67	18.80	EA	-
29	LMC_SC1	CG LEO 333 03 00 -70 03 16.8	03:33:03.00	-70:03:16.8	437.666	-42.17822	1.113260	-433.67346	18.73	0.83	0.30	0.77	18.67	18.69	EA	-
30	LMC_SC1	CG LEO 333 04 23 -70 16 13.1	03:33:04.23	-70:16:13.1	479.737	36.32470	6.977370	-441.26483	16.88	0.16	0.30	0.13	16.83	17.79	EA	-
31	LMC_SC1	CG LEO 333 06 15 -69 52 32.0	03:33:06.15	-69:52:32.0	489.048	60.16938	5.487330	-437.61490	19.39	1.54	0.32	0.37	19.24	19.83	EA	-
32	LMC_SC1	CG LEO 333 08 13 -70 01 12.0	03:33:08.13	-70:01:12.0	518.822	-40.99223	0.877760	-436.16928	18.48	0.61	0.30	0.40	18.47	18.38	EA	-
33	LMC_SC1	CG LEO 333 08 59 -69 51 30.2	03:33:08.59	-69:51:30.2	522.166	61.66181	1.319240	-434.49937	19.11	1.46	0.49	0.31	19.13	19.46	EA	-
34	LMC_SC1	CG LEO 333 10 22 -69 46 18.9	03:33:10.22	-69:46:18.9	536.399	69.66693	2.643300	-437.80026	17.89	0.43	0.30	0.36	17.70	18.38	EA	-
35	LMC_SC1	CG LEO 333 11 23 -70 21 33.3	03:33:11.23	-70:21:33.3	568.646	18.54398	3.222480	-433.47968	19.33	1.36	0.30	0.48	19.37	19.79	EA	-
36	LMC_SC1	CG LEO 333 11 63 -69 46 00.2	03:33:11.63	-69:46:00.2	532.788	73.01847	2.144280	-436.27341	18.62	0.67	0.43	0.60	18.61	18.93	EA	ecc
37	LMC_SC1	CG LEO 333 11 89 -69 46 53.0	03:33:11.89	-69:46:53.0	537.314	68.79499	6.194370	-432.65093	19.21	1.47	0.30	0.43	19.04	19.62	EA	-
38	LMC_SC1	CG LEO 333 12 11 -70 11 24.8	03:33:12.11	-70:11:24.8	573.304	33.29444	0.937130	-439.10728	18.37	0.39	0.31	0.34	18.38	18.36	EA	-
39	LMC_SC1	CG LEO 333 12 02 -70 07 02.3	03:33:12.02	-70:07:02.3	579.838	36.62860	3.394410	-434.74613	17.24	0.38	0.49	0.30	17.20	17.18	EA	-
40	LMC_SC1	CG LEO 333 14 43 -70 11 08.8	03:33:14.43	-70:11:08.8	603.296	24.98369	2.389720	-433.36033	18.43	0.80	0.49	0.30	18.37	18.46	EA	-
41	LMC_SC1	CG LEO 333 14 03 -70 10 03.3	03:33:14.03	-70:10:03.3	603.700	33.21483	1.703680	-436.13387	13.92	0.18	0.33	0.11	16.90	16.94	EA	EB/EW/ELL
42	LMC_SC1	CG LEO 333 17 37 -69 36 03.2	03:33:17.37	-69:36:03.2	630.339	33.90101	23.913340	-443.18483	18.11	1.02	0.30	0.31	18.06	19.47	EA	-
43	LMC_SC1	CG LEO 333 18 09 -69 53 02.6	03:33:18.09	-69:53:02.6	646.393	37.01929	4.637010	-432.73410	16.17	0.90	0.30	0.26	16.16	16.17	EA	-
44	LMC_SC1	CG LEO 333 20 14 -70 20 23.0	03:33:20.14	-70:20:23.0	676.300	30.24697	33.031330	-433.69769	19.93	3.33	0.46	0.17	17.37	18.71	EA	-
45	LMC_SC1	CG LEO 333 20 79 -69 54 27.7	03:33:20.79	-69:54:27.7	673.067	37.86338	1.339130	-436.41648	17.38	0.39	0.30	0.33	17.33	17.37	EA	-
46	LMC_SC1	CG LEO 333 21 09 -70 17 43.3	03:33:21.09	-70:17:43.3	686.834	24.13402	6.108740	-437.02623	18.40	0.63	0.30	0.40	18.33	19.32	EA	-
47	LMC_SC1	CG LEO 333 23 28 -70 08 03.3	03:33:23.28	-70:08:03.3	710.338	38.18887	7.187330	-436.73287	16.81	0.80	0.30	0.13	16.78	16.94	EA	-
48	LMC_SC1	CG LEO 333 26 23 -70 31 14.1	03:33:26.23	-70:31:14.1	733.480	-49.4843	2.940330	-433.34469	17.46	0.43	0.30	0.13	17.43	17.33	EA	-
49	LMC_SC1	CG LEO 333 26 04 -69 46 04.2	03:33:26.04	-69:46:04.2	741.367	72.92347	3.346780	-434.60946	19.14	1.18	0.30	0.48	19.08	19.63	EA	-
50	LMC_SC1	CG LEO 333 27 33 -69 32 03.3	03:33:27.33	-69:32:03.3	733.273	61.30116	4.634330	-431.62319	19.13	1.37	0.31	0.33	18.99	19.86	EA	-
51	LMC_SC1	CG LEO 333 27 33 -69 36 36.3	03:33:27.33	-69:36:36.3	733.630	68.7617	1.881640	-436.28478	16.82	0.22	0.30	0.16	16.82	17.77	EA	-
52	LMC_SC1	CG LEO 333 28 26 -70 31 42.1	03:33:28.26	-70:31:42.1	792.021	38.8908	1.410280	-434.97334	18.83	0.84	0.30	0.77	18.84	19.13	EA	-
53	LMC_SC1	CG LEO 333 32 31 -70 20 43.2	03:33:32.31	-70:20:43.2	827.473	19.80933	0.834800	-434.93369	18.74	0.72	0.30	0.32	18.39	18.80	EA	-
54	LMC_SC1	CG LEO 333 33 36 -70 13 02.4	03:33:33.36	-70:13:02.4	833.261	30.94330	1.730140	-436.77013	18.66	0.70	0.30	0.64	18.37	18.88	EA	-
55	LMC_SC1	CG LEO 333 33 28 -70 24 10.9	03:33:33.28	-70:24:10.9	839.462	14.79432	1.477300	-434.48173	18.13	0.72	0.30	0.71	18.08	18.31	EA	-
56	LMC_SC1	CG LEO 333 33 31 -70 23 29.2	03:33:33.31	-70:23:29.2	863.209	12.90170	1.338860	-434.46014	17.98	0.29	0.30	0.17	17.93	18.03	EA	-
57	LMC_SC1	CG LEO 333 33 88 -69 44 38.1	03:33:33.88	-69:44:38.1	837.662	71.62363	3.279440	-433.33190	17.49	0.21	0.49	0.18	17.43	17.88	EA	-
58	LMC_SC1	CG LEO 333 36 23 -69 53 11.6	03:33:36.23	-69:53:11.6	863.397	33.84366	1.737140	-436.92413	18.89	1.03	0.31	0.70	18.80	19.44	EA	-
59	LMC_SC1	CG LEO 333 38 33 -69 39 26.3	03:33:38.33	-69:39:26.3	887.382	79.64427	2.294200	-437.66603	17.82	0.37	0.30	0.34	17.80	17.94	EA	-
60	LMC_SC1	CG LEO 333 38 31 -70 02 48.8	03:33:38.31	-70:02:48.8	893.317	-47.54113	3.632330	-438.38663	17.71	0.31	0.30	0.24	17.69	17.69	EA	-
61	LMC_SC1	CG LEO 333 40 37 -69 34 33.4	03:33:40.37	-69:34:33.4	916.499	37.										

Table 1: Definition of Eclipse Stages

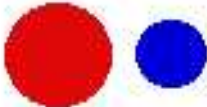
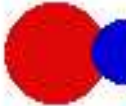
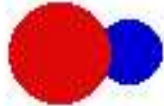




STAGE	RANGE	APPEARANCE
No Eclipse	$\rho > (R_1 + R_2)$	
Shallow Eclipse	$(R_1 + R_2) > \rho > \sqrt{R_1^2 - R_2^2}$	 OR 
Deep Eclipse	$\sqrt{R_1^2 - R_2^2} > \rho > (R_1 - R_2)$	 OR 
Annular or Total Eclipse	$\rho < (R_1 - R_2)$	 OR 

Figure 22: condition

E. J code to get the physical parameters of the stars.

Binary maker

Binary maker is commercially available software package developed by david Bradstreet (Eastern colleg eof pensylvania) to visualize light and radial velocity curves and the appearance of the system itself with varying phase.

- 1) Light curve can tell us star shapes, and various kinds of surface brightness and the orientation information
- 2) Light curve can provide a picture of binary with an unknown scale, while radial velocitycurve can provide absolute scale but no picture.
- 3) Velocity curves of both the stars are needed to compute the scalling information, although radial velocities for just one of the stars give useful, but incomplete information.

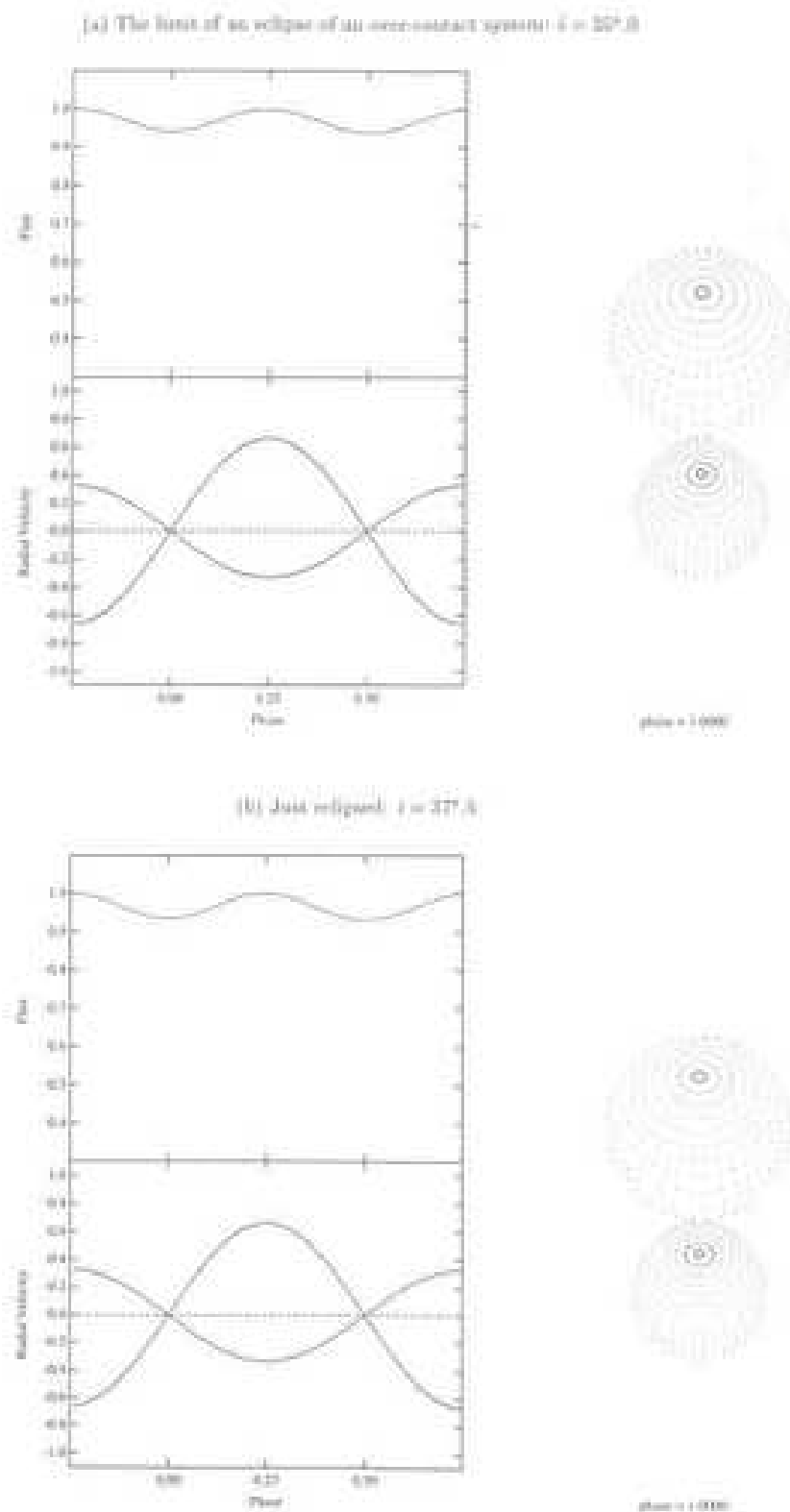


FIGURE F.1. The limit of an eclipse of an over-contact system.

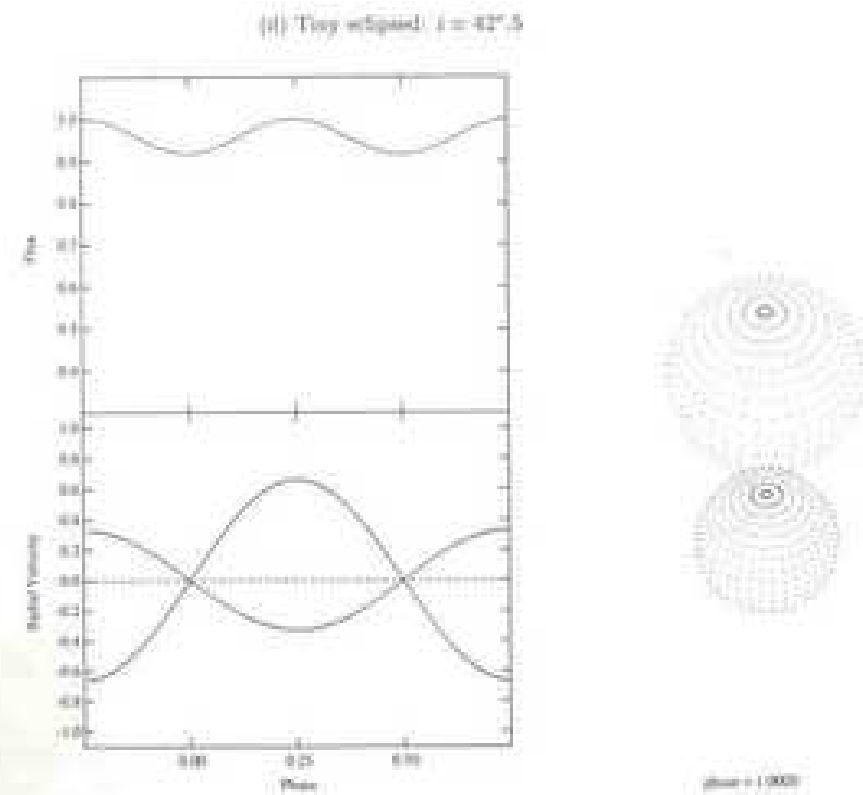
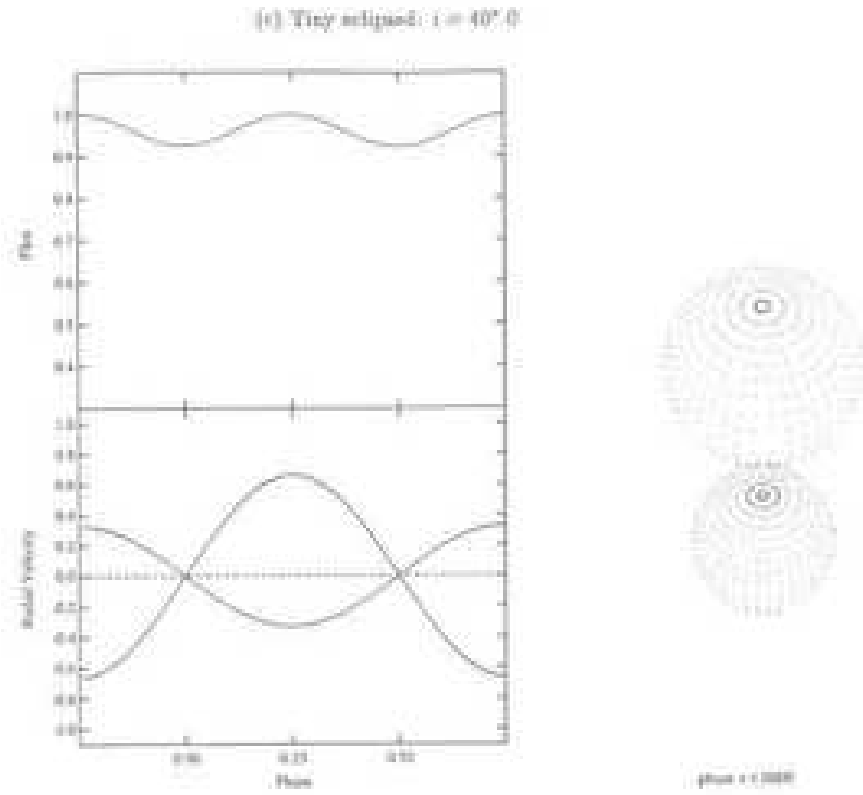
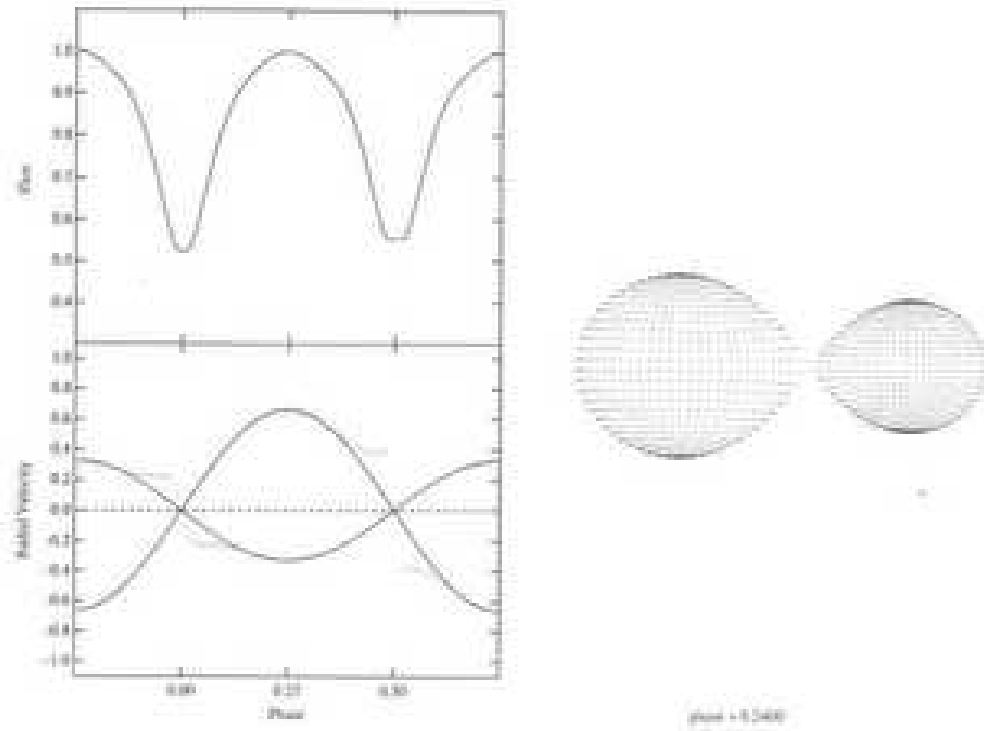


FIGURE F.2. Shallow eclipses.

(e) Just eclipse: $i = 90^\circ$, b without third light



(f) Deep eclipse: $i = 90^\circ$, b including third light $\ell_3 = 0.5$

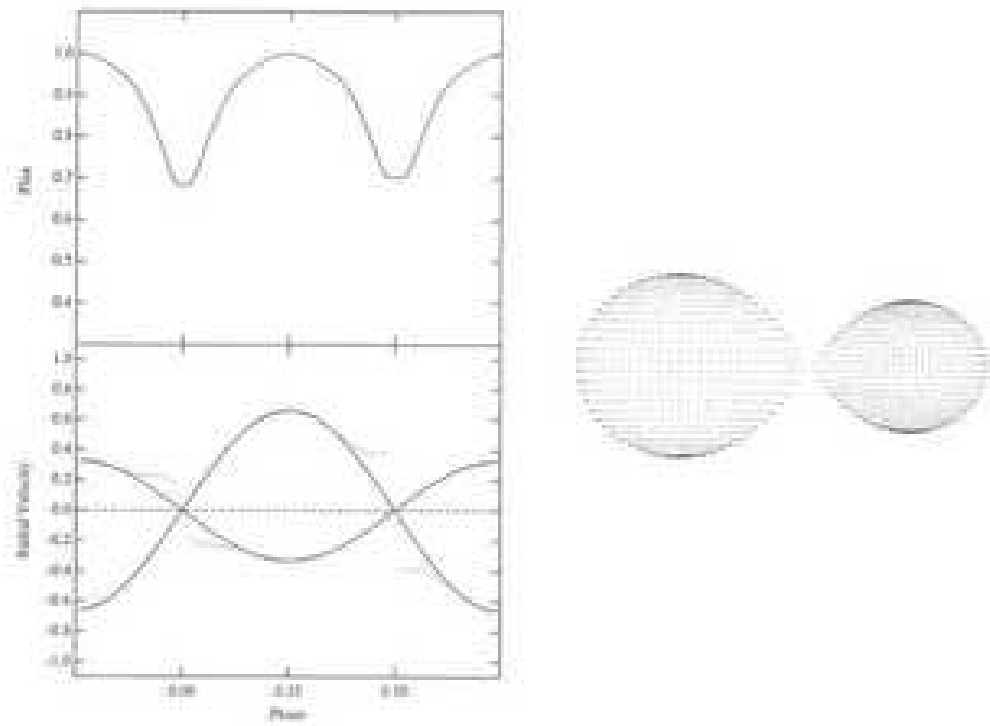


FIGURE F.3. Deep eclipses.

Figure 25: Light curves deep eclipses

Input data for Binmaker code:

- (1) latitude grid No
- (2) longitude grid No
- (3) mass ratio
- (4) Potentials as a Omega: potential 1 and Potential 2
- (5) Wave length
- (6) Temp1
- (7) Temp2
- (8) g1
- (9) g2
- (10) x1
- (11) x2
- (12) reflection 1
- (13) reflection 3
- (14) L3
- (15) spots details

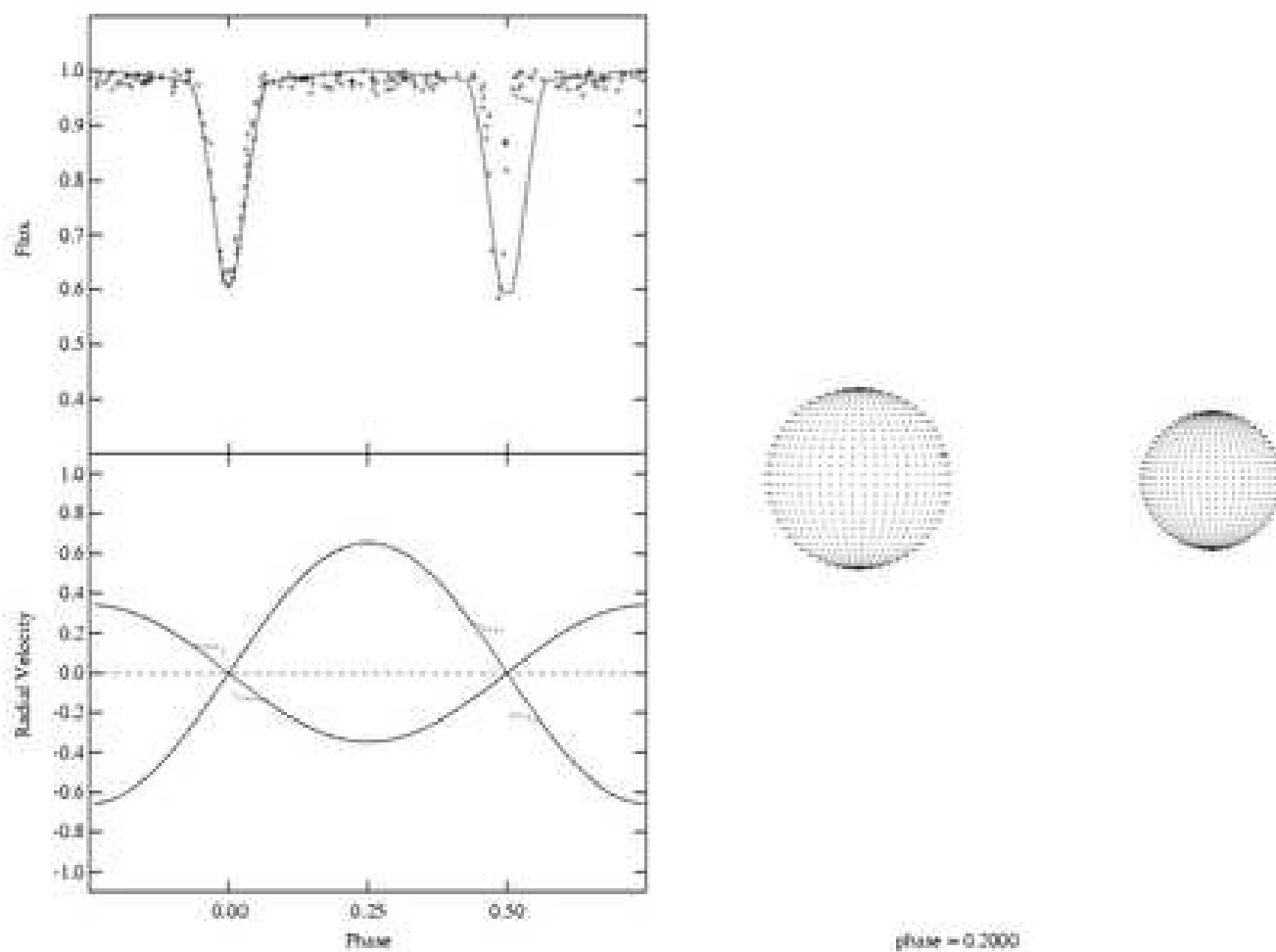


Figure 26: Synthetic light curve

For deriving the physical parameters of each system we can fix two crucial parameters like temperature and the mass ratio (as derived from the spectroscopy). The temperature is always assumed as that approximate for the spectral type and the mass ratio will be derived from the radial velocity curve. Since we can get multiple solution of the system. That is way we apply Binmaker2 code, where we can get global minimum parameters of the system and secondly it is independent of correlations between parameters of describing the system.

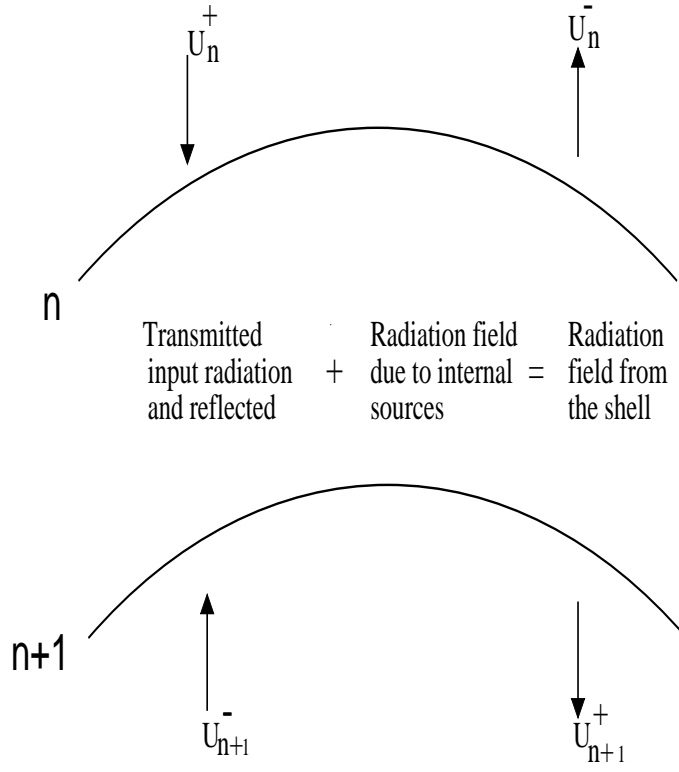


Figure 27: Schematic diagram of diffuse radiation field

$$\begin{pmatrix} \mathbf{U}_{n+1}^+ \\ \mathbf{U}_n^- \end{pmatrix} = \begin{pmatrix} \mathbf{t}(n+1, n) & \mathbf{r}(n, n+1) \\ \mathbf{r}(n+1, n) & \mathbf{t}(n, n+1) \end{pmatrix} \begin{pmatrix} \mathbf{U}_n^+ \\ \mathbf{U}_{n+1}^- \end{pmatrix} + \begin{pmatrix} \Sigma_{n+\frac{1}{2}}^+ \\ \Sigma_{n+\frac{1}{2}}^- \end{pmatrix} \quad (25)$$

The \mathbf{r} and \mathbf{t} matrices and the vectors Σ^\pm are the internal sources which can be expressed in terms of the matrices.

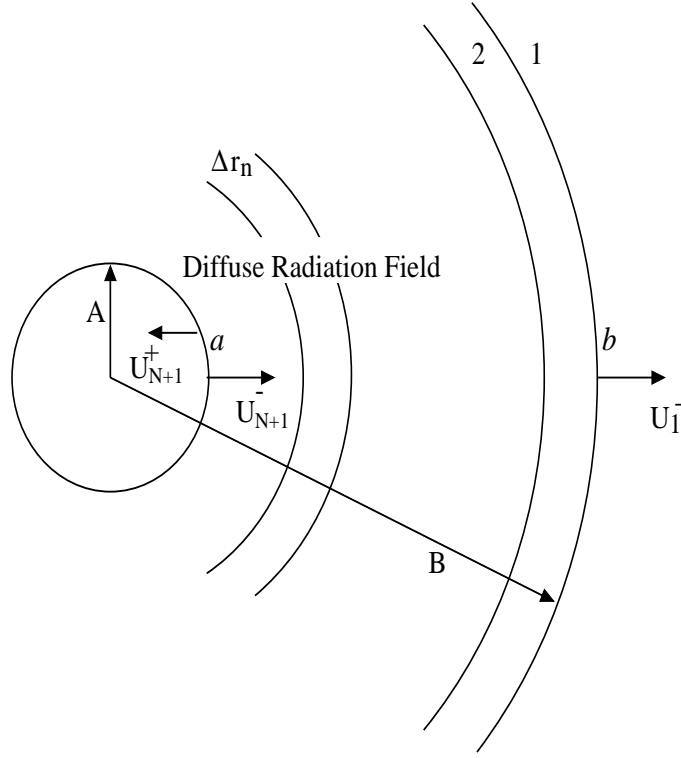


Figure 28: Schematic diagram of interaction principle

a) Classification based on the shape of the light curve

E Eclipsing binary systems. These are binary systems with orbital planes so close to the observer's line of sight (the inclination i of the orbital plane to the plane orthogonal to the line of sight is close to 90 deg) that both components (or one of them) periodically eclipse each other. Consequently, the observer finds changes of the apparent combined brightness of the system with the period coincident with that of the components' orbital motion.

EA Algol (Beta Persei)-type eclipsing systems. Binaries with spherical or slightly ellipsoidal components. It is possible to specify for their light curves the moments of the beginning and end of the eclipses. Between eclipses the light remains almost constant or varies insignificantly because of reflection effects, slight ellipsoidality of components, or physical variations. Secondary minima may be absent. An extremely wide range of periods is observed, from 0.2 to $i = 10000$ days. Light amplitudes are also quite different and may

reach several magnitudes.

EB Beta Lyrae-type eclipsing systems. These are eclipsing systems having ellipsoidal components and light curves for which it is impossible to specify the exact times of onset and end of eclipses because of a continuous change of a system's apparent combined brightness between eclipses; secondary minimum is observed in all cases, its depth usually being considerably smaller than that of the primary minimum; periods are mainly longer than 1 day. The components generally belong to early spectral types (B-A). Light amplitudes are usually ≥ 2 mag in V.

EW W Ursae Majoris-type eclipsing variables. These are eclipsers with periods shorter than 1 days, consisting of ellipsoidal components almost in contact and having light curves for which it is impossible to specify the exact times of onset and end of eclipses. The depths of the primary and secondary minima are almost equal or differ insignificantly. Light amplitudes are usually ≥ 0.8 mag in V. The components generally belong to spectral types F-G and later.